

A Reservoir-based Model for Human-like Perception of Complex Rhythm Pattern

Zhongju Yuan¹, Geraint Wiggins^{2,3*}, Dick Botteldooren^{1*}

¹WAVES Research Group, Ghent University, Ghent, Belgium

²AI Lab, Vrije Universiteit Brussel, Belgium

³EECS, Queen Mary University of London, UK

zhongju.yuan@ugent.be, geraint.wiggins@vub.be, dick.botteldooren@ugent.be

Abstract—Rhythm is a fundamental aspect of human behaviour, present from infancy and deeply embedded in cultural practices. Rhythm anticipation is a spontaneous cognitive process that typically occurs before the onset of actual beats. While most research in both neuroscience and artificial intelligence has focused on metronome-based rhythm tasks, studies investigating the perception of complex musical rhythm patterns remain limited. To address this gap, we propose a hierarchical oscillator-based model to better understand the perception of complex musical rhythms in biological systems. The model consists of two types of coupled neurons that generate oscillations, with different layers tuned to respond to distinct perception levels. We evaluate the model using several representative rhythm patterns spanning the upper, middle, and lower bounds of human musical perception. Our findings demonstrate that, while maintaining a high degree of synchronization accuracy, the model exhibits human-like rhythmic behaviours. Additionally, the beta band neuronal activity in the model mirrors patterns observed in the human brain, further validating the biological plausibility of the approach.

Index Terms—Rhythm perception, Dynamic system, Reservoir computing, Time series prediction

I. INTRODUCTION

WHEN a child sings a nursery rhyme or a musician performs Mozart, the neural mechanisms underlying the perception and production of music pose intriguing questions for cognitive neuroscience [1]. The interaction between auditory and motor systems has garnered significant attention. For instance, playing a musical instrument, such as the drums, requires precise coordination between the auditory signal (the musical note or beat) and the motor action (the movement of the arm to strike the drum pad). Three fundamental motor control functions are essential for performing rhythmic patterns: timing, sequencing, and movement organization. Accurate timing governs the rhythmic structure, while sequencing and organization are crucial for executing each note in the rhythmic sequence.

These motor control functions correspond to different levels of metric rhythmic pattern perception. Metric rhythmic patterns are typically divided into three levels: Tatum, Tactus, and Measure. The Tatum represents the smallest unit of subdivision, corresponding to the fundamental frequency that governs the timing of events within the rhythmic pattern [2]. The Meter, rooted in the perception and production of the pulse

or tactus, is flexible across a range of frequencies [3]. Across cultures, music unfolds within a higher-order metric structure, creating musical expectations that enable individuals to predict and organize future motor behaviours [4], [5], [6]. Both the tactus and measure levels contribute to the sequencing and organization of rhythmic patterns.

Rhythm perception and production involve several brain regions in a hierarchical manner [2], [7] as well. Neuropsychological and neuroimaging studies have revealed distinct pathways originating in the primary auditory cortex and projecting to various targets [8], [9]. Some neurons are specifically tuned to the fundamental frequency of complex tones [10]. Research suggests that rhythmic features are processed along separate streams [11], [12]. Additionally, the basal ganglia and supplementary motor area (SMA) play critical roles in interval timing, with the former focusing on longer timescales (over one second) and the latter specializing in shorter timescales (milliseconds) [1], [13]. The pre-SMA and SMA are implicated in organizing complex movement sequences [14], [15], [16], while the premotor cortex is associated with the production of complex motor sequences and motor prediction [17], [18], [19]. Importantly, both rhythm perception and production engage motor regions of the brain [17], [20], [21], [22].

Despite significant progress in neuroscience, many previous studies have focused primarily on simple rhythms, often requiring participants to tap a single finger to a constant beat [23]. While these tasks have provided insights into basic perceptual and motor timing properties [24], it remains uncertain whether neural models derived from these tasks are applicable to complex rhythmic patterns. Recent experiments have explored the perception and reproduction of more intricate musical rhythms, revealing increased involvement of the dorsal premotor cortex (dPMC), lateral cerebellar hemispheres, and prefrontal cortex [25], [26], [27], [28]. Studies also highlight the role of beta-range activity (15–30 Hz) in temporal predictions [29], [30], [31]. However, it remains unclear whether these neural changes directly relate to the temporal complexity of rhythms or are influenced by other factors, such as sequence complexity or the predictability of rhythmic structures during motor performance.

To address these gaps, we propose a physics-inspired dynamic framework comprising multiple hierarchical layers corresponding to distinct levels of rhythmic perception. This framework aims to advance our understanding of human per-

*Corresponding author: Geraint Wiggins, Dick Botteldooren.

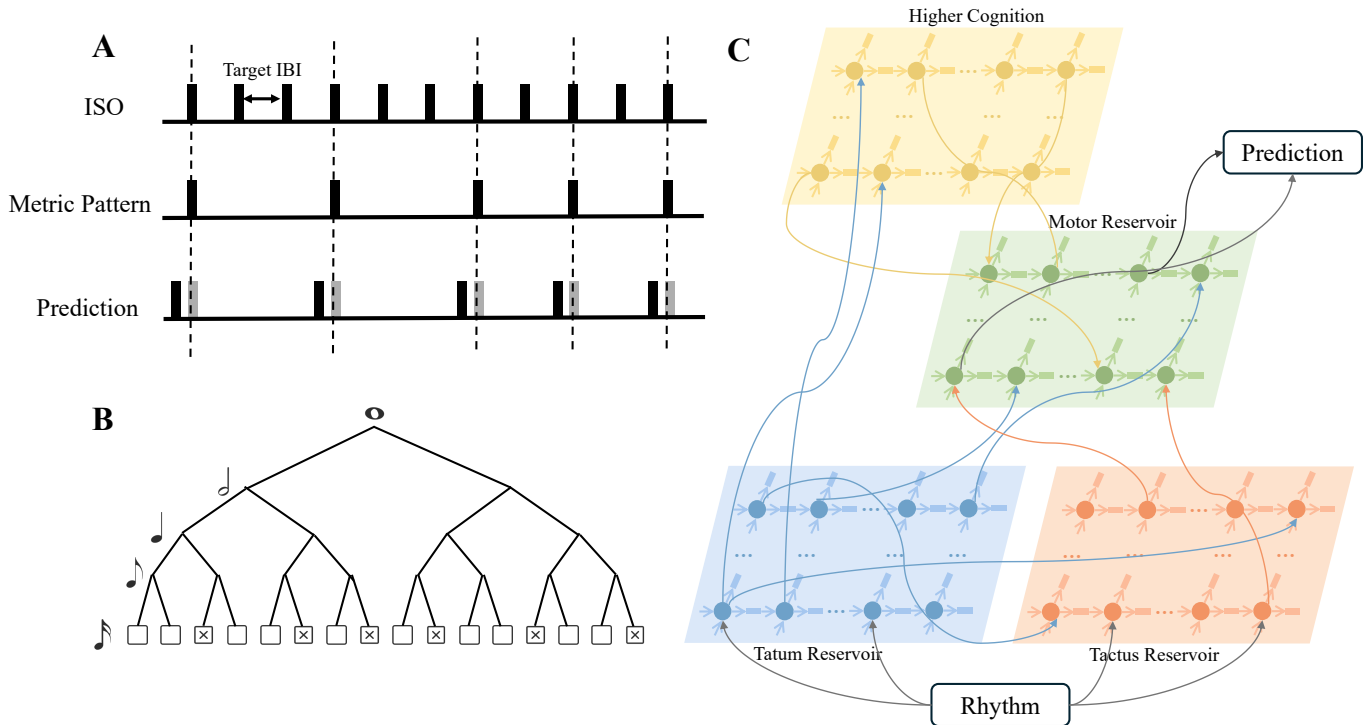


Fig. 1: **Schematic representation of rhythm structure and the architecture of the proposed model for complex rhythm pattern prediction.** (A) Definitions used in the rhythm illustration. All complex patterns are derived from an isochronous (ISO) rhythm, characterized by equal inter-beat intervals (IBI), with the target IBI serving as the smallest time unit in the complex pattern. The complex pattern is a metric pattern, where each "on-beat" aligns with a beat in the ISO. Predictions are made for beats occurring 200 ms before the "on beat" in the metric pattern. (B) Hierarchical musical perception structure, as described by Vuust et al. [32], is illustrated. Each metric level is recursively subdivided into equally spaced sub-units at the next lower level, defining the metric salience of positions within the rhythmic framework. The tactus lies at the midpoint of this structure. (C) The architecture of the proposed model, showing the flow of information within the system. The model consists of four distinct layers, each with specialized functions, with the Motor Layer responsible for generating the predictions.

ception of complex metric rhythmic patterns. Specifically, we hypothesize that manipulating rhythmic properties at various levels will suffice to induce motor engagement during rhythm-predictive coding tasks.

II. RELATED WORK

Music is a universal aspect of human culture, characterized by rhythmic patterns that listeners follow for movement and performers rely on for synchronization [33]. Recent research suggests that nonlinear oscillations, which are intrinsic to brain dynamics, play a critical role in rhythm entrainment, with resonant interactions contributing to temporal synchronization [34], [35].

Studies on musical rhythm processing highlight the role of neural oscillations in auditory-motor synchronization [36], identifying key brain regions such as the basal ganglia for beat-based rhythms, the cerebellum for processing complex sequences [37], and the dorsal premotor cortex for coordinating motor actions [38]. Neural pathways originating in the auditory cortex exhibit frequency-tuned responses [8], [9], [10]. Additionally, EEG studies have linked specific frequency activations to binary and ternary rhythms [23], [39], yet the modeling of oscillator networks to handle complex rhythmic

patterns remains underexplored. These findings provide a biological foundation for rhythm perception models.

Musical rhythm perception involves identifying periodic pulses within temporally complex sound sequences. Human participants demonstrate rhythmic synchronization with these pulses, which is commonly evaluated by finger-tapping experiments [40], [25]. This synchronization reveals that beat perception is a predictive process, as taps align closely with beats, typically within tens of milliseconds, reflecting the brain's capacity for precise temporal predictions [41], [42].

Beats are often structured into patterns that create hierarchical periodicities, such as march-like patterns with strong beats every two pulses or waltz-like patterns with strong beats every three pulses [3], [43], [44]. In rhythm theory, the smallest time unit, known as the tatum, forms the basis of these patterns [2]. The tactus, or "strong" beat, is typically a multiple of the tatum [2]. Humans perceive rhythms across a wide temporal range, with the strongest rhythmic responses occurring within 400–1200 ms intervals [3].

An important finding in the neuroscience of rhythm perception is the engagement of motor regions during beat processing, even in the absence of overt movement. Key areas include the premotor cortex (PMC), basal ganglia, and supplementary

motor area (SMA) [37], [45], [46], [47]. Functional connectivity between auditory and motor regions, which is stronger in musicians than non-musicians, underpins this process [46]. A cortico-subcortical network involving the putamen, SMA, and PMC is critical for analyzing temporal sequences and predicting beats [48], [49].

Complex rhythms, especially those with non-integer ratios (e.g., 3:2), challenge auditory-motor synchronization, leading to greater variability and reduced accuracy in beat detection [50]. Neural measures, such as decreased EEG power and ERP amplitudes, suggest that increasing rhythmic complexity impacts both behavioral performance and neural entrainment. These insights motivate this study's exploration of the motor system's role in auditory timing and rhythm prediction.

III. METHODS

In this paper, we introduce the concept of rhythm within the context of isochronic and metrically complex patterns (see Fig. 1(a)). Isochronic rhythms are characterized by a fixed basic inter-beat interval (IBI), whereas metric rhythms exhibit a hierarchical structure that captures the subtleties of more complex rhythmic patterns, as illustrated in Fig. 1(b). We selected these rhythmic patterns at the measure level, which repeat periodically throughout the trial. The predictive coding task was designed to capture these patterns and predict the onset of each beat 200 ms in advance, reflecting the tendency of humans to anticipate the beat slightly before the actual event occurs.

We implemented a four-layer neural network architecture to perform the complex pattern predictive coding task, as shown in Fig. 1(c). The network comprises the Tatum Layer, Tactus Layer, Higher Cognition Layer, and Motor Layer. Each layer is responsible for distinct aspects of rhythm processing and prediction. The Tatum Layer detects the smallest rhythmic unit, the basic IBI, while the Tactus Layer identifies the slower underlying rhythm. The Higher Cognition Layer serves as long-term memory, and the Motor Layer generates motor responses based on predictions informed by long-term memory.

A. Reservoir structure

All layers operate within a unified structural framework governed by the same core set of equations:

$$\begin{aligned} \mathbf{h}_{t+1} &= (1 - \alpha)\mathbf{h}_t + \alpha f(\mathbf{W}_{in}\mathbf{x}_t + \mathbf{W}\mathbf{h}_t + \xi_t), \\ \hat{\mathbf{y}}_t &= \mathbf{W}_{out}\mathbf{h}_t, \end{aligned} \quad (1)$$

where \mathbf{W} is a sparse matrix representing the internal connectivity of the layer, \mathbf{W}_{in} is the input weight matrix, and \mathbf{W}_{out} is the output weight matrix. The parameter α is the leakage rate. The function $f(\cdot)$ is a non-linear activation function, with $\tanh(\cdot)$ used in this study. \mathbf{x}_t represents the input vector at time step t , \mathbf{h}_t is the hidden state of the layer at time step t , and $\hat{\mathbf{y}}_t$ is the corresponding output. The model aims to predict $\mathbf{y}_t = \mathbf{x}_{t+n}$, where n is the number of steps into the future, defined as $\Delta t = n\delta t$, with δt being the simulation time step.

Conventionally, the weight matrix of the layer, \mathbf{W} , the input weight matrix, \mathbf{W}_{in} , and the bias matrix, \mathbf{b}_t , are randomly generated at each time step. In this work, we introduce \mathbf{W}_{bias} ,

which includes Gaussian noise, ξ_t , regenerated at each time step. The weight matrix \mathbf{W} is defined using the following equations:

$$\begin{aligned} \frac{\partial p}{\partial t} + c^2 \nabla \mathbf{o} &= 0, \\ \frac{\partial \mathbf{o}}{\partial t} - k\mathbf{o} + \nabla p &= 0, \end{aligned} \quad (2)$$

where c is the wave speed, k is the damping factor (or amplification factor if negative), and p and \mathbf{o} represent pressure and velocity, respectively.

Using the finite-difference time-domain (FDTD) model with a staggered grid, central differences, and explicit time-stepping, the discretized form of these equations is given by (Eq. 3):

$$\begin{aligned} p_{i,j}(t + \delta t) &= p_{i,j}(t) + c_{i,j}^2 \delta t \frac{o_{x,i+1,j} - o_{x,i,j}}{\delta x} \\ &\quad + c_{i,j}^2 \delta t \frac{o_{y,i,j+1} - o_{y,i,j}}{\delta y}, \\ o_{x,i,j}(t + \delta t/2) &= \frac{1 - k_{i,j}\delta t/2}{1 + k_{i,j}\delta t/2} o_{x,i,j}(t - \delta t/2) \\ &\quad + \frac{\delta t}{\delta x(1 + k_{i,j}\delta t/2)} (p_{i,j} - p_{i-1,j}), \end{aligned} \quad (3)$$

where the indices i and j refer to spatial locations, and the time dependence has been omitted on the right-hand side for brevity. A similar discretization applies for o_y . To ensure stability, the Courant number, which relates δt to δx and δy , must remain below 1.

The two groups of unknowns can be interpreted as two types of artificial neurons within the reservoir, as illustrated in Fig. 1. The primary neuron is denoted as $p_{i,j}$, while the intermediate neuron is labeled as $o_{x,i,j}$ or $o_{y,i,j}$. These neurons can be grouped into a hidden state matrix, \mathbf{x} , as shown in Eq. 1. Since p and \mathbf{o} are coupled locally and sparsely, the coupling matrix, \mathbf{A} , derived from Eq. 3, will also exhibit sparsity.

The weight matrix, \mathbf{W} , of the reservoir is computed as:

$$\mathbf{W} = \frac{\mathbf{A} - (1 - \alpha) \cdot \mathbf{I}}{\alpha}, \quad (4)$$

where \mathbf{I} is the identity matrix. In this formulation, the reservoir update equations (Eq. 4) closely resemble the FDTD update equations, implying strong symmetry constraints on the \mathbf{W} matrix. The local value of c determines the responsiveness of the p -neuron to inputs from neighboring o -neurons. Together with the coupling to its neighbors, this can result in local resonances, where small c values correspond to low-frequency resonances, a phenomenon akin to physical systems.

By introducing a gradient in c on top of random values, a reservoir with both slow (low-frequency resonances) and fast (high-frequency resonances) dynamics can be achieved, as shown in Fig. 1. The variable k controls the information propagation speed between p -neurons via the o -neurons. Increasing k results in more heavily damped resonances.

The output weights for each layer are optimized using gradient descent to facilitate the accurate learning and prediction

of complex rhythmic patterns. The weight update is governed by the following gradient equation:

$$\mathbf{W}_{out} = \mathbf{W}_{out} - \gamma \frac{\partial l_{MSE}}{\partial \mathbf{W}_{out}}, \quad (5)$$

where γ denotes the learning rate, and l_{MSE} represents the Mean Square Error for layer l . This process is iterated over multiple steps to refine the weights.

B. Framework Structure

Algorithm 1 Learn to predict a complex rhythm pattern

```

1: Init: pattern sequence, trigger sequence, epoch,
   sequence length, learning step, update step, iterative step,
   learning rate  $\gamma$ 
2: for  $n$  in epoch do
3:   for  $l$  in length(pattern_sequence) do
4:      $\hat{y}_l^{hc} = \text{sigmoid}(W_{out}^{hc} h_l^{hc})$ 
5:      $\mathcal{L}_{BCE} = -\frac{1}{N} \sum_{l=1}^N \left[ \text{pattern\_sequence}_l \log(\hat{y}_l^{hc}) \right. \\ \left. + (1 - \text{pattern\_sequence}_l) \log(1 - \hat{y}_l^{hc}) \right]$ 
6:      $W_{out}^{hc} \leftarrow W_{out}^{hc} - \text{ADAM}(\nabla_{W_{out}^{hc}} \mathcal{L}_{BCE})$ 
7:   end for
8: end for
9: for  $t$  in sequence_length do
10:   $h_t^{tatum} = (1 - \alpha)h_{t-1}^{tatum} + \alpha f(W_{in}^{tatum} x_t^{tatum} \\ + W^{tatum} h_{t-1} + \xi_t^{tatum})$ 
11:   $h_t^{tactus} = (1 - \alpha)h_{t-1}^{tactus} + \alpha f(W_{in}^{tactus} x_t^{tactus} \\ + W^{tactus} h_{t-1} + \xi_t^{tactus})$ 
12:  if  $t \geq \text{start\_time}$  then
13:    if  $\hat{y}^{motor} = 0$  then
14:       $W^{motor} \leftarrow W^{motor\_ori}$ 
15:    else
16:       $W^{motor} \leftarrow W^{motor\_damp}$ 
17:    end if
18:  end if
19:   $h_t^{motor} = (1 - \alpha)h_{t-1}^{motor} + \alpha f(W_{in}^{motor} x_t^{motor} \\ + W^{motor} h_{t-1} + \xi_t^{motor})$ 
20:  if  $t \leq \text{start\_time}$  then
21:    if  $t \leq \text{update\_step}$  then
22:      if  $t \% \text{update\_step}$  is 0 then
23:        for  $i$  in iterative_step do
24:          Note: * means the tatum, tactus,
25:          and motor.
26:           $l_{MSE}^* = \frac{(\hat{\mathbf{y}}^* - \mathbf{y}^*)^2}{\text{update\_step}}$ 
27:           $W_{out}^* \leftarrow W_{out}^* - \gamma \frac{\partial l_{MSE}^*}{\partial W_{out}^*}$ 
28:        end for
29:      end if
30:    end if
31:  end if
32:   $\hat{y}_t^{tatum} = W_{out}^{tatum} h_t^{tatum}$ 
33:   $\hat{y}_t^{tactus} = W_{out}^{tactus} h_t^{tactus}$ 
34:   $\hat{y}_t^{motor} = W_{out}^{motor} h_t^{motor}$ 
35: end for

```

The connection structure between input and output weights varies across layers, allowing each layer to generate distinct outputs while remaining synchronized with the rhythmic input. This layer-wise differentiation enhances rhythm-based predictions. The full learning algorithm is provided in Algorithm 1.

The rhythmic pattern is not pre-encoded in the system's memory, akin to how a novel rhythm would be unfamiliar to a person. Consequently, the system requires time to learn and synchronize with the pattern by predicting at each beat. During the initial steps, denoted as `update_step`, the model updates the output weights W_{out} for all layers. To minimize computational load, updates to W_{out} are restricted to a limited number of iterations within each fixed update step, employing gradient descent with a learning rate γ , as described in Algorithm 1.

The Tatum Layer is designed to capture the smallest rhythmic interval, or tatum, from the complex input pattern. The output of this layer represents the tatum, and to enhance the accuracy of on-beat event predictions, a forward-shifted target of 200 milliseconds is used to update the output weights. This forward shift aligns the Tatum Layer's output with the anticipated beat locations, improving its predictive performance. Importantly, the output weights of other layers remain unchanged for prediction purposes. As shown in Fig. 1(c), the input to the Tatum Layer, x_t^{tatum} , represents the rhythm at time step t .

Human perception of rhythm typically requires slower processing, addressed by the Tactus Layer. This layer processes the Tatum Layer output in conjunction with the original complex pattern. The input to the Tactus Layer at time step t , x_t^{tactus} , is given by $\hat{y}_t^{tatum} + x_t^{tatum}$. As illustrated in Fig. 1, the reservoir structure incorporates fast and slow ends to capture fast and slow frequency envelopes, respectively. By inputting these signals into the fast end of the Tactus Layer and connecting the readout layer only to the slow end, the Tactus Layer captures the hierarchical structure of rhythm, which is essential for predicting slower rhythmic patterns with high accuracy.

A single-layer reservoir is insufficient to capture complex rhythmic structures due to its limited memory capacity. Therefore, we introduce the Higher Cognition Layer, which serves as a long-term memory, learning and storing rhythmic patterns. This layer is implemented as a state-space model and is activated by peaks in the Tatum Layer output. When a peak is detected, a trigger signal activates the Higher Cognition network, enabling it to predict whether the next beat will be present or absent. Peaks are identified when $\hat{y}_{t-1}^{tatum} \geq \hat{y}_{t-2}^{tatum}$ and $\hat{y}_{t-1}^{tatum} \leq \hat{y}_t^{tatum}$, with \hat{y}_{t-1}^{tatum} marked as the event occurrence time. Upon receiving the trigger at position l , the hidden state h_l^{hc} is updated, and the output weight W_{out}^{hc} infers the probability of a missing or present beat after one inter-beat interval (IBI). During training, W_{out}^{hc} is updated by minimizing the Binary Cross Entropy loss, with the learning of W_{out}^{hc} beginning before the other layers engage in prediction. This process mirrors human participants learning a novel rhythm, requiring time to listen and comprehend the structure, thereby enhancing the anticipation of rhythmic variations, including the prediction of missing beats.

Following the prediction from the Higher Cognition Layer,

the neuron connections within the Motor Layer, denoted as W^{motor} , are adjusted. The Motor Layer integrates input from both the Tatum and Tactus Layers, where x_t^{motor} is $\hat{y}_t^{tatum} + \hat{y}_t^{tactus}$. Its output weights are updated to align with the predictions, enabling the network to capture complex rhythmic structures and generate appropriate motor responses.

The Motor Layer output sometimes omits beats based on fundamental isochronous rhythms, necessitating intervention from the Higher Cognition Layer. When a missing beat is predicted, the Higher Cognition Layer modulates the damping effect on the Motor Layer, preventing beat omission.

Damping is controlled by dynamically adjusting the connection matrix of the Motor Layer. When the Higher Cognition Layer predicts a missing beat, the damping matrix k is increased to a stronger negative value, generating the connectivity matrix W^{motor_damp} . After a predefined period, the matrix reverts to its original state W^{motor_ori} , allowing normal rhythmic behavior to resume.

After completing the learning stage, the output weights W_{out}^* across all layers were fixed. At the designated prediction start time, the Higher Cognition Layer initiated the Motor Layer's connectivity state switching. This matrix switching substantially modulated neuronal activity. We recorded neural responses across several common rhythmic patterns and compared these with human EEG spectra. The observed similarities between the neural activity produced by our model and that in human brain rhythms suggest that our network effectively replicates key aspects of human rhythmic perception.

IV. RESULTS

We propose a four-layer, physics-inspired reservoir model designed to simulate human motor engagement during music rhythm prediction tasks. Given the hierarchical nature of music rhythms, the model is structured to align with the inherent organization of rhythm. The four layers—Tatum Layer, Tactus Layer, Motor Layer, and Higher Cognition Layer—reflect this hierarchy, as illustrated in Fig. 1(C). For further details, please refer to the Materials and Methods section.

To evaluate the performance of the proposed model on complex rhythmic patterns, we selected a diverse set of binary-encoded sequences, with each pattern represented by a combination of 0s and 1s. These sequences were based on an isochronous (ISO) rhythm with a fixed inter-beat interval (IBI) serving as the fundamental unit, or "tatum", of each pattern, as shown in the top row of Fig. 1(A). The metric patterns are represented by a binary encoding, a value of 1 signifies an on-beat event aligned with the rhythm, whereas a value of 0 indicates an off-beat event, as shown in the second row of Fig. 1(A), where vertical bars represent 1, and the omitted beats in the tatum correspond to 0. The final outputs are intended to predict these on-beats, represented by the black vertical bars in the third row of Fig. 1(A). The experimental set included six patterns: three simpler ones (101001, 101000, and 10101001) and three more challenging ones (1001001010, referred to as "Mission Impossible"; 10110010, referred to as "Normal Rock"; and 101010100100, referred to as "Normal Jazz"), and a irregular one 10010.

Model performance was tested across various tempos, represented by beats per minute (BPM): 60, 100, and 140 BPM. These values correspond to IBIs of 1,000 ms, 600 ms, and 428.6 ms, respectively. The tempo range was selected based on findings in [3], which demonstrate that beat perception is robust across a wide range of tempi. The chosen BPM values include a lower bound (60 BPM), an upper bound (140 BPM), and a mid-range value (100 BPM). As the model operates at the granularity of the tatum (the smallest rhythmic unit), the IBIs in our experiments correspond to 500 ms, 300 ms, and 214 ms, respectively.

The proposed four-layer model was designed to predict complex rhythmic patterns. The input to the model consists of a time series characterized by peaks that follow a repeating pattern at a fixed BPM. The model's final output from the Motor Layer predicts the signal 200 ms ahead of the input. Prediction errors were calculated by comparing the model's outputs with target signals, enabling an accurate assessment of its performance.

The Tatum Layer, responsible for capturing the smallest subdivisions with stable IBIs, was pretrained on a dataset comprising 1,000 generated samples. These samples featured beat frequencies ranging from 66 to 168 BPM, with 25% of the dataset consisting of non-rhythmic signals to enhance diversity. Each sample was 30 seconds long with a 6 ms time step, and starting and ending points were randomly selected to ensure broad representation. The remaining layers were trained from scratch without pretraining.

Results Measurements

To evaluate the motor behaviour generated by the model, three key metrics are employed, as detailed in this section. Resultant Vector Length and Mean Asynchrony are used to assess the model's performance for beats corresponding to those in the given complex patterns. An additional overall metric, Tempo Matching Accuracy, is used to evaluate the synchronization quality across the entire sequence.

Relative Phase Angle: All measurements are derived from an error metric that quantifies synchronization based on the phase difference between the real rhythm and the motor output beat onsets. Specifically, the timing of the real rhythm and the motor-generated beats are denoted as T and B , respectively.

Since the model may miss beats or introduce extra beats compared to the mathematically strict rhythm, many standard metrics fail to provide an accurate evaluation. To address this, the closest peak for each beat B_n in B is identified within T , resulting in a matched tapping beat list M . Additionally, the index of each matched peak in T is collected in an index list I . This approach ensures that synchronization is evaluated based on the closest corresponding beats, allowing for a more robust and meaningful assessment.

For all beats in B , the relative phase angles are calculated using Eq.(6)[51], [52]:

$$\phi = 360 \times \frac{M_n - B_n}{B_{n+1} - B_n}, \quad (6)$$

where M_n represents the n -th beat in the matched tapping beat list M , and B_n denotes the n -th beat in the given rhythm. A

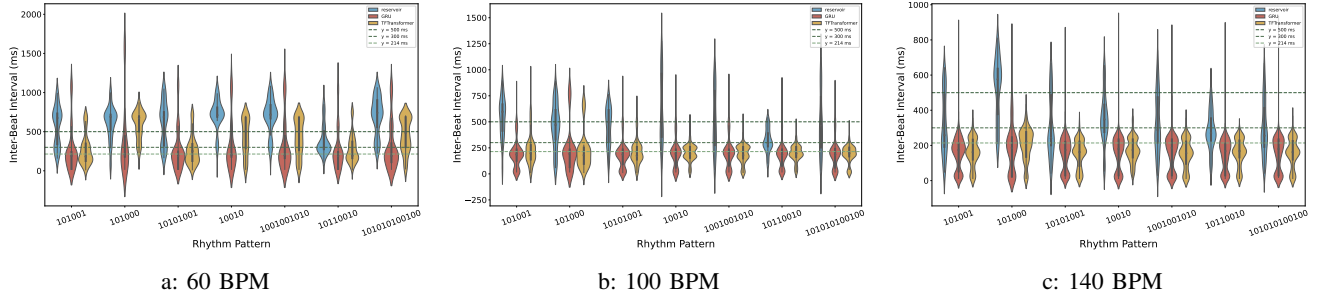


Fig. 2: **Comparison of Tatum Inter-Beat Interval (IBI) Distributions Across Different Models After Pretraining.** All models were pre-trained on the same single-channel rhythmic dataset, and IBIs were computed for each rhythm pattern at three distinct frequencies. The horizontal dashed lines indicate the corresponding tatum IBIs.

negative phase angle indicates that the model’s generated beat occurs ahead of the corresponding metronome beat, whereas a positive phase angle suggests that the model’s beat lags behind the target beat in the rhythm.

Resultant Vector Length: The resultant vector length quantifies the stability of relative phase angles over time. A unimodal distribution corresponds to a high resultant vector length, while uniform or bipolar distributions result in a low value [53]. The resultant vector length, R , is calculated using the relative phase angles as shown in Eq. (7):

$$R = \left| \frac{1}{N} \sum_{n=1}^N e^{i\phi M_n} \right|, \quad (7)$$

where N is the number of peaks in the given rhythm signal. The value of R ranges from 0 to 1, with 1 indicating perfect synchronization over time and 0 representing the absence of synchronization.

Mean Asynchrony: Mean asynchrony measures the average timing difference between the model’s tap onsets and the corresponding onsets of the given complex rhythm, expressed in milliseconds. It is computed as follows:

$$\text{Mean Asynchrony} = \frac{1}{N} \sum_{n=1}^N (M_n - B_n), \quad (8)$$

where M_n and B_n denote the n -th beats in the matched tapping beat list and the given rhythm, respectively.

Tempo Matching Accuracy: Tempo matching accuracy assesses how well the overall tempo of the model’s actions aligns with the tempo of the given rhythm, based on inter-beat intervals (IBIs). Inter-beat deviation (IBD) is defined as the mean difference between the model’s IBIs and those of the given rhythm [52].

To calculate IBD, the timing of matched beats in M is used, indexed in T . If the model generates an extra beat at $I_n - 1$, the interval $T_{I_n} - T_{I_n - 1}$ will be smaller than $M_n - M_{n-1}$. Consequently, the error compared to $B_n - B_{n-1}$ will increase, making this metric effective for evaluating overall tempo matching. The IBD is calculated as follows:

$$\text{IBD} = \frac{1}{N} \sum_{n=2}^N \frac{|(B_n - B_{n-1}) - (T_{I_n} - T_{I_n - 1})|}{B_n - B_{n-1}}. \quad (9)$$

Zero-shot Learning for Tatum Layer

The Tatum Layer is designed to capture the underlying smallest time unit (tatum) and make predictions ahead of time. For training, the input consists of randomly generated rhythm patterns with varying frequencies, while the target is the corresponding tatum signal shifted 200 ms ahead of the input beat onsets. The training set includes 5,000 pairs of 30-second rhythm signals. Three models were trained on this dataset: Gated Recurrent Unit (GRU) [54], Temporal Fusion Transformer (TFTransformer) [55], and the proposed Tatum Layer. All models were trained for 50 epochs, aiming to minimize the mean squared error (MSE) between their outputs and the target signals.

The evaluation results are illustrated through the inter-beat interval (IBI) distributions for each sequence. As depicted in Fig. 2, none of the models successfully captured the precise tatum intervals or consistently generated their multiples. The expected tatum IBIs are 500, 300, and 214 ms. Based on the mean IBI values provided in Fig. 4, the mean error ratios—calculated as the percentage difference between the models’ mean IBIs and the expected values—are 34.63%, 25.93%, and -50.85% for the GRU, TFTransformer, and our proposed model, respectively.

As the models were trained on rhythm patterns spanning diverse frequencies, and the test set features both unseen patterns and frequencies, this task is inherently classified as a zero-shot learning problem.

To address this challenge, the model leverages auxiliary information—such as the semantic representations of rhythm—and learns to generalize across variations in frequency and timing. Meta-learning steps are incorporated to enhance the model’s generalization capabilities. Fig. 3 illustrates the inter-beat interval (IBI) distributions of the Tatum Layer’s output before and after meta-learning, highlighting its improved alignment with the expected tatum intervals.

For most patterns under 60 BPM, the mean IBI after adaptation closely approximates the target of 500ms. However, for the patterns 101000 and 101000, the mean IBI reaches approximately 1.5 times the target value. In Fig. 3(A), the tatum distribution for 101000 exhibits two peaks at 542.0 ms and 958.2 ms, corresponding to the target value and its double. Similarly, the pattern 101000 shows peaks at 630.8

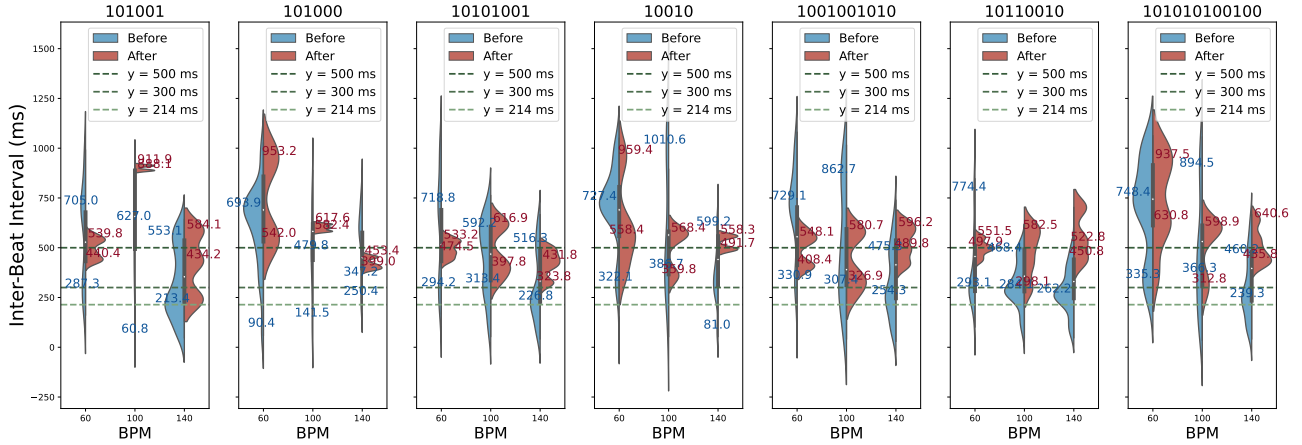


Fig. 3: Comparison of Tatum Inter-Beat Interval Distributions Before and After Zero-shot Learning of Our Model. After a brief input adaptation phase at the start, the output weight matrix is fixed. Following this adaptation, the IBIs of each pattern are calculated and compared to their pre-adaptation values across three distinct frequencies. The violin plots highlight two prominent peaks, with horizontal dashed lines indicating the corresponding tatum IBIs.

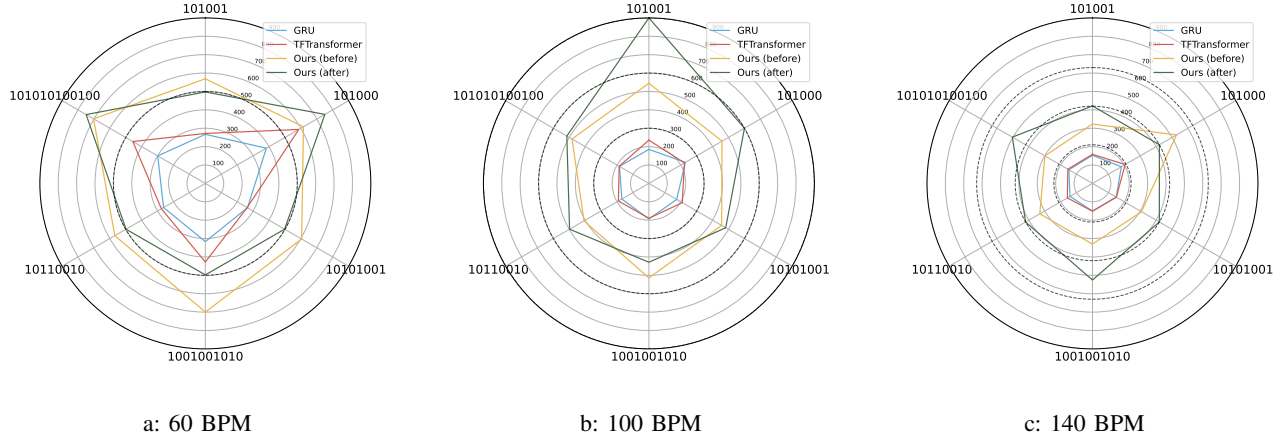


Fig. 4: Comparison of Mean IBIs from the Tatum Layer Output Across Different Models and Pre- vs. Post-Zero-Shot Learning for Our Model Across Various Patterns and Frequencies. Panels (A, B, C) display the mean IBIs across different frequencies, respectively. For each frequency, the mean output IBIs of all patterns are measured for three models, as well as for our model before and after zero-shot learning. The mean values for each model are represented by distinct colored lines in the corresponding radar plot, while the tatum IBIs and their multiples are depicted as black dashed hollow circles in each panel.

ms and 937.5 ms, which align with the target value and double its length.

For patterns under 100 BPM, except for 101001 and 101000, the other patterns display two significant peaks in their IBI distributions, as shown in Fig. 3(B). The lower peaks are observed at 397.8 ms, 326.9 ms, 343.6 ms, and 312.8 ms, while the upper peaks are at 616.9 ms, 580.7 ms, 580.4 ms, and 598.9 ms, respectively. The lower peaks are close to the target, and the upper peaks align with approximately double the target length. For 101001 and 101000, the model predicts intervals closer to triple and double the target length, respectively.

For patterns under 140 BPM, most mean intervals approximate double the target length, which is consistent with human perception thresholds around 250 ms. Notably, patterns such as

101000 and 101010100100 exhibit lower peaks at 421.2 ms and 435.8 ms, and upper peaks at 596.2 ms and 640.6 ms, respectively. The lower peaks correspond closely to double the target length, while the upper peaks align with triple the target length.

Pattern 10010 presents a challenge for human recognition, as the tactus becomes more ambiguous due to alternating between double and triple tatum. For the Tatum Layer, at a frequency of 60 BPM, the distribution exhibits two prominent peaks at 558.4 ms and 959.4 ms. At 100 BPM, the distribution shows peaks at 359.8 ms and 568.4 ms. The lower peaks correspond closely to the target tatum values of 500 ms and 300 ms, while the higher peaks align with double tatum. At the faster tempo of 140 BPM, the tatum distribution shifts,

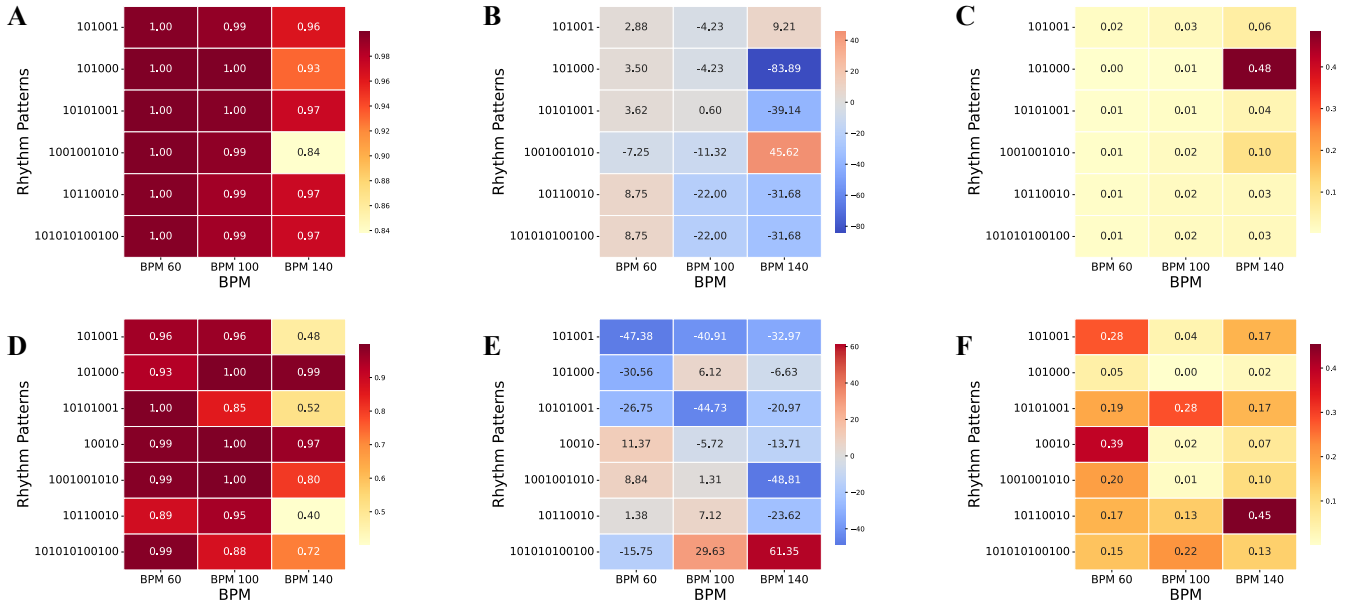


Fig. 5: Comparison of Tactus and Motor Layer Outputs Across Patterns and Frequencies. Panels (A, B, C) display the measurements for the Tactus Layer outputs, while Panels (D, E, F) present the corresponding measurements for the Motor Layer outputs. Synchronization Strength (range: 0–1) is shown in Panels (A, D). Mean Asynchrony (unit: ms) is illustrated in Panels (B, E). Inter-Beat Deviation (IBD, range: 0–1) is depicted in Panels (C, F).

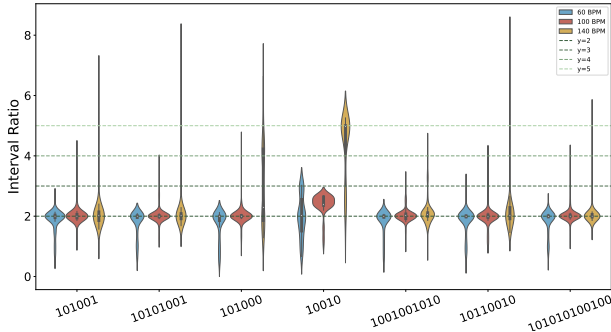


Fig. 6: Tactus IBI distribution aligned with the target smallest time unit. The inter-beat intervals (IBIs) generated by the Tactus Layer for all rhythmic patterns, evaluated at three distinct frequencies, are normalized by their respective target IBIs. The y-axis represents the resulting distribution, illustrating that the Tactus Layer effectively captures the slower meter in hierarchical rhythm perception.

revealing two peaks at 491.7 ms and 558.3 ms, which are near the values for double and triple tatum, respectively.

In summary, after applying meta-learning, the Tatum Layer’s output IBI distributions align well with the target smallest time unit or its multiples, demonstrating the model’s capacity to adapt to rhythmic variations effectively.

Analysis of Tactus Layer Output

Humans cannot directly perceive and track musical rhythms solely based on a series of tatum [2]. At a minimum, the perception of a metrical pattern requires a tactus level coordinated with at least one additional organizational level.

To simulate this human capability, we introduce a dedicated layer called the Tactus Layer. Since the tactus cannot emerge independently, the output of the Tatum Layer is used as input to the Tactus Layer. Furthermore, to capture the hierarchical structure inherent in rhythmic patterns, the complex rhythmic input is also provided to this layer. During the initial 12 seconds, the output weights of the Tactus Layer are updated based on the corresponding target output.

The beats within each rhythm are identified, and the IBIs are calculated accordingly. The IBI distributions across different patterns and beats per minute (BPM) are visualized in Fig. 6. The x-axis represents the rhythmic patterns, while the y-axis indicates the multiples of the target smallest time unit corresponding to each IBI. Horizontal reference lines at double, triple, quadruple, and quintuple multiples are included to illustrate how the tactus IBI distributions vary with frequency changes.

As shown in Fig. 6, the Tactus Layer successfully captures double-digit beats in most cases. However, the upper tails of the distributions tend to elongate as frequency increases, indicating a bias toward slower tactus levels. For example, in the pattern 101000, at 140 BPM, the model often captures a quadruple-multiple beat. In a more ambiguous case, 10010, the changes in the tactus IBI distribution are more pronounced. At the low frequency of 60 BPM, the distribution exhibits two distinct peaks at double and triple the target smallest time unit. As the frequency increases to 100 BPM, the tactus tends to divide the pattern length into intervals approximately 2.5 times the target unit. At 140 BPM, the model captures the entire pattern using quintuple multiples, reflecting a significant adaptation to the faster rhythm.

To elucidate the tactus patterns, we present circular dot

plots in Fig. 7. In these visualizations, 2π represents the total duration of the pattern digits multiplied by the smallest time unit, with uniform angular spacing between the green lines reflecting the tatum.

Each blue dot represents a peak detected in the output of the Tactus Layer. The angular position of each dot indicates its relative phase within the rhythmic pattern, while the radial distance conveys the most recent inter-beat interval (IBI). These visualizations emphasize the alignment between the detected tactus and the underlying rhythmic patterns.

Fig. 7(a, b, c) illustrate three common rhythmic patterns: 101001 and 101000, which are three-beat patterns, and 10101001, a four-beat pattern. Corresponding measurements of motor behaviour for these patterns are shown in the first row of Fig. 5. The tactus beats are well-aligned with the target patterns, as evidenced by the synchronization strength, which exceeds 0.9 for all patterns across different frequencies. Relative phase errors are minimal, although a slight decline in synchronization strength is observed at 140 BPM.

From Fig. 7(a, b, c), the Tactus Layer output dots cluster clearly around the two-digit pattern 10, though clusters for 101000 in Fig. 7(c) appear noisier at 140 BPM compared to other frequencies. The mean asynchrony and inter-beat deviation (IBD) corroborate this observation in Fig. 7(c), indicating larger distance errors in motor behaviour at 140 BPM. For the overall match rate, the pattern 101000 shows lower accuracy due to occasional misalignment, with the Tactus Layer detecting a four-time cycle instead. This misalignment is consistent with the distribution shown in Fig. 6. Notably, larger absolute mean asynchronies are negative, indicating that the motor behaviour anticipates the beat by triggering earlier than the target timing. These deviations are not necessarily detrimental, as they remain systematic and aligned with the rhythmic pattern.

Fig. 7(e, f, g) explore more complex patterns: 10010010, 10110010, and 101010100100. Measurements of motor behaviour for these patterns are shown in the second row of Fig. 5. While the Tactus Layer output beats are similarly well-aligned with the target patterns, synchronization strengths tend to be slightly lower than those observed for three-beat and four-beat patterns, reflecting the increased complexity. At 140 BPM, the model exhibits greater variability, with slightly larger absolute mean asynchronies. However, as these asynchronies are predominantly negative, they indicate early motor responses rather than errors. The IBD values remain close to zero, confirming that the Tactus Layer reliably identifies repeated two-digit patterns such as 10, even in more complex rhythmic scenarios. This consistency highlights the robustness of the model in synchronizing with rhythmic patterns across varying levels of difficulty.

For the hard pattern 10010, the tactus exhibits greater ambiguity, with inter-beat intervals that are not consistently equal. As shown in Fig. 7(d), at slower tempos, the tactus beats tend to cluster around double and triple tatum. Additionally, other clusters emerge at positions where the pattern attempts to divide into three roughly equal intervals, aligning with human perceptual tendencies. The other frequencies results shown in the figure is well aligned with the numerical results.

Analysis of The Motor Layer Output

The Motor Layer provides the final instructions for striking the beat, synthesizing inputs from both the tatum and Tactus Layers. During the initial 24 seconds, the output weights of the Motor Layer are dynamically adjusted to optimize alignment with the target rhythmic predictions.

To visualize the motor instructions, we present circular dot plots in Fig. 7. These plots represent 2π as the total duration of the rhythmic pattern, scaled by the smallest time unit. Dark green dashed lines mark the relative phases of on-beats (i.e., '1's), while light green dotted lines indicate off-beats (i.e., '0's). The uniform angular spacing between the green lines reflects the tatum, providing a temporal framework for the Motor Layer's outputs.

In these visualizations, red dots represent beats detected from the Motor Layer's output, while blue dots indicate peaks from the Tactus Layer. The angular position of each dot corresponds to its relative phase within the rhythmic pattern, and its radial distance encodes the most recent inter-beat interval (IBI). These visualizations emphasize the alignment between the outputs of the reservoirs and the underlying rhythmic structure.

The beat onset visualizations further illustrate the alignment between the Motor Layer output and the target rhythmic patterns. Fig. 7 presents seven representative patterns, while the corresponding measurements of motor behaviour for these patterns are summarized in Fig. 5. The results demonstrate that the Motor Layer achieves precise synchronization with these patterns, maintaining high accuracy across varying rhythmic complexities.

The mean asynchronies reported in Fig. 5 are approximately 40 ms, with predominantly negative values, indicating that the model slightly anticipates the beat by producing outputs marginally ahead of the real beat. This behaviour aligns with observations in embodied systems, where such anticipation is a common phenomenon.

Given the variability in motor output, identifying overarching trends is challenging. To address this, we analyze each rhythmic pattern individually, focusing on frequency-dependent variations.

For the pattern 101001, shown in Fig. 7(a), synchronization strength at 140BPM is the lowest among the three tested frequencies when considering only beats that align correctly with the pattern. As illustrated in Fig. 7(A.a), motor-generated beats synchronize well with the first two 1's but lead the timing for the third 1'. Additionally, Fig. 7(C.a) shows an extra peak generated by the motor, caused by the tactus beat not aligned with the 1's in the pattern. This misalignment drifts the third 1' off its correct timing. The mean asynchrony remains consistently negative across frequencies without transitioning to another digit. Notably, the inter-beat deviation (IDB) at 60 BPM is the highest, attributed to the extra peak generated by the motor-tactus interaction.

For the pattern 101000, shown in Fig. 7(c), synchronization strength exceeds 0.9 for all tested frequencies, considering only properly matched beats. The mean asynchrony values are consistently small and negative, with the largest being -30.56 . All IDBs are below 0.05, indicating no extra peaks generated

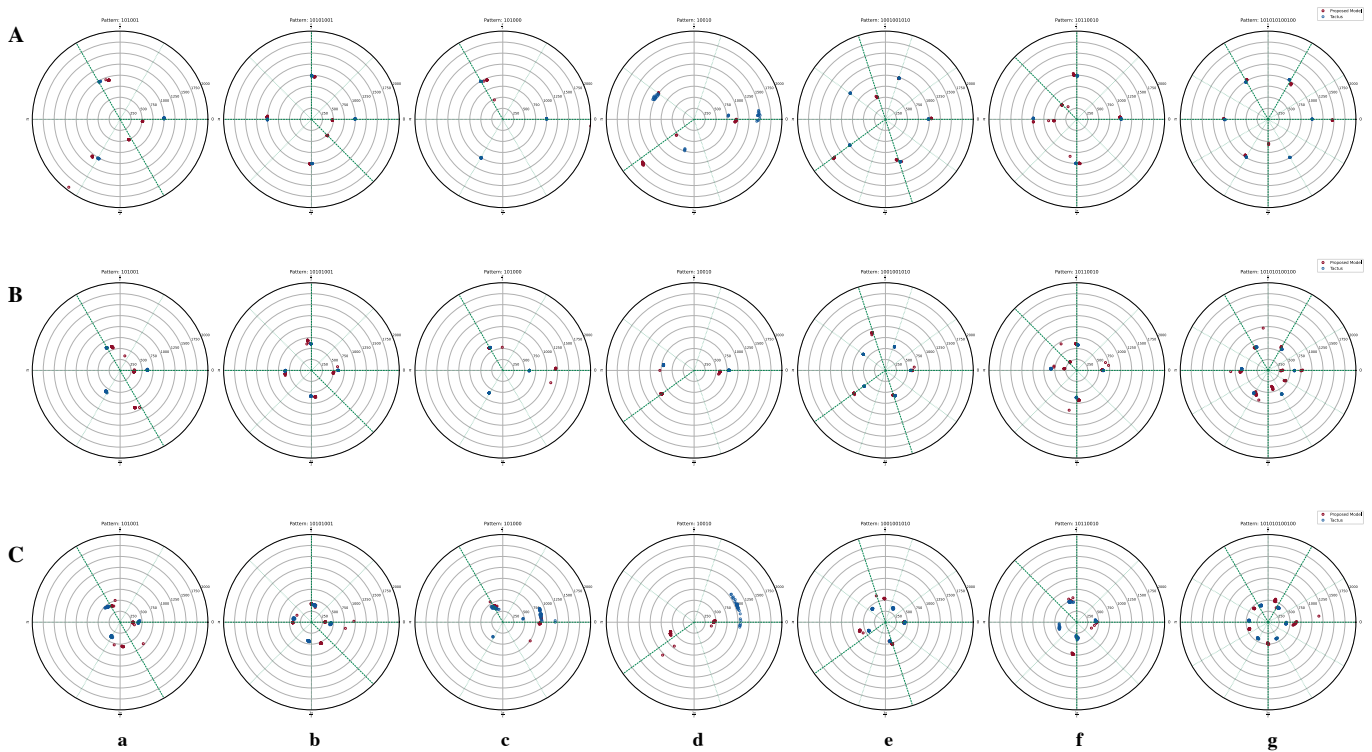


Fig. 7: Visualization of rhythmic patterns highlighting the alignment of Tactus Layer and Motor Layer output beats across the entire sequence. Each row represents a specific frequency across all patterns, with panels (A, B, C) corresponding to 60, 100, and 140 BPM, respectively. Subplots within the same row depict variations in performance across different patterns for the given frequency. In each subplot, the Tactus Layer and Motor Layer outputs are displayed. Hollow circles indicate beats omitted by both layers, where the circle’s angle represents the phase shift relative to the cycle (pattern digit length \times smallest time unit) and the radial distance indicates the interval between consecutive beats. The dark green dashed line from the circle’s center marks onset beats ($'1$'s) in the pattern, while the light green dashed line denotes offset beats ($'0$'s).

by the motor. This observation aligns with the motor behaviour depicted in Fig. 7(c).

For the pattern 10101001, shown in Fig. 7(b), the behaviour is similar to pattern 101001. Synchronization strength at 140BPM is the lowest among the frequencies tested, while other frequencies exhibit stronger synchronization. From Fig. 7(A.b), motor-generated beats match the first two 1’s but lead the timing for the third 1’. As shown in Fig. 7(C.b), the motor generates an additional peak, driven by the tactus beat that does not coincide with the 1’s in the pattern. Consequently, the third 1’ drifts away from its proper timing. The mean asynchrony remains negative across all frequencies, while the IDB at 60BPM is the highest, driven by the motor-induced extra peak.

For the pattern 1001001010 shown in Fig. 7(e), the synchronization strength remains consistently above 0.8 across all tested frequencies. However, at 140 BPM, the synchronization strength is the lowest, while other frequencies exhibit stronger synchronization. The mean asynchrony also shows a larger error at 140 BPM, supporting the conclusion derived from the synchronization strength measurement. For the inter-digital beats (IDBs), an example at 60 BPM shows a value of 0.1999, indicating the generation of extra peaks by the model. Specifically, as illustrated in Fig. 7(A.e), the motor generates

an extra peak at the third digit of the pattern, driven by the tactus.

For the pattern 10110010 shown in Fig. 7(f), the synchronization strength remains consistently above 0.88 at lower frequencies. The tactus is reliably captured; however, the third ‘1’ in the pattern does not align with the tactus, leading to ambiguous motor behaviour at this position. The nature of the motor behaviour varies across different tempi. At 60 and 100 BPM, the synchronization strength approaches 1, and the mean asynchrony is smaller compared to higher tempi. However, the inter-beat deviations (IDBs) exceed 0.1. As illustrated in Fig. 7(A.f) and Fig. 7(B.f), additional beats are omitted at the fourth digit in the pattern, a phenomenon that aligns with the observed tactus. At faster tempi, such as 140 BPM, the motor beats at the ambiguous position exhibit noticeable drift. As shown in Fig. 7(C.f), the red dots deviate from the second dark green line and cluster around the tactus beat. This drift is attributed to the difficulty in distinguishing the two consecutive ‘1’s at higher speeds, causing the model to omit one. Consequently, correct beats are infrequently generated at the third ‘1’ in the pattern, resulting in increased mean asynchrony and larger IDBs.

For the pattern 101010100100 shown in Fig. 7(g), the synchronization strength decreases as the BPM increases. This

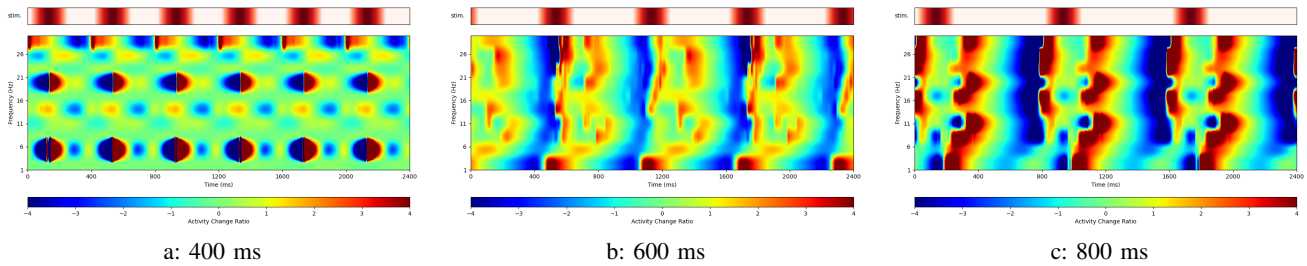


Fig. 8: Neural Activity in Motor Layer Neurons. The hidden states of all p neurons were recorded as the model processed the corresponding example. A Hilbert transform was applied along the time dimension to obtain the envelope of neural activities in 3 Hz intervals, ranging from 0 to 30 Hz. The figure illustrates the rate of change in these neural activities, with corresponding beat markers displayed above each spectrum.

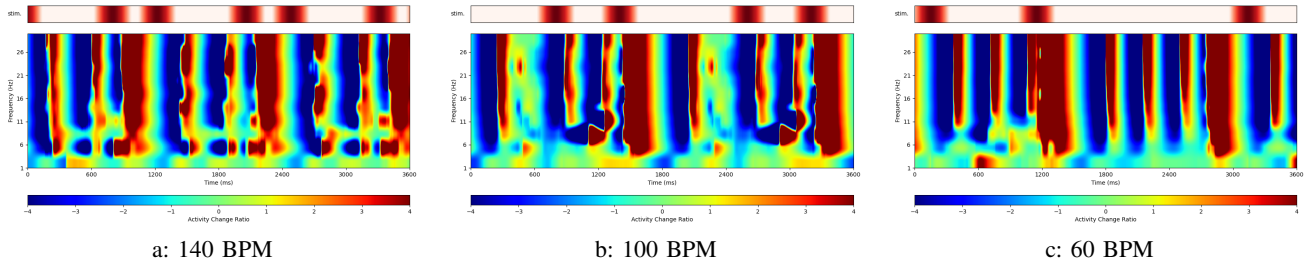


Fig. 9: Neural Activity in Motor Layer Neurons of pattern 101000 with three distinct frequencies. The hidden states of all p neurons were recorded as the model processed the corresponding example. A Hilbert transform was applied along the time dimension to obtain the envelope of neural activities in 3 Hz intervals, ranging from 0 to 30 Hz. The figure illustrates the rate of change in these neural activities, with corresponding beat markers displayed above each spectrum.

trend can be attributed to the increasing level of ambiguity at faster tempi, as commonly observed in jazz music. At 60 BPM, the synchronization strength is nearly 1, and the mean asynchrony is -15.75 ms, indicating that the motor taps slightly ahead of the beat. However, the IDB is 0.1479 due to an extra peak at the ninth digit, as shown in Fig. 7(A.g). These results suggest that the Tatum Layer captures 12 tatum peaks for this pattern, simplifying the prediction task for the higher cognitive layers. At 100 and 140 BPM, the variance increases, with mean delays of 29.6308 ms and 61.3548 ms, respectively. The clusters in Fig. 7(B.g) and Fig. 7(C.g) are noisier than those at 60 BPM. At 100 BPM, the IDB increases to 0.2154 due to ambiguous tatum representation, as the Tatum Layer fails to capture all 12 tatum peaks and instead combines some smaller time units. At 140 BPM, while the model successfully captures all beat onsets, it exhibits a mean delay of 61.3548 ms, reflecting a degradation in timing precision.

For the challenging pattern 10010, the results are presented in Fig. 5 and Fig. 7(d). The Motor Layer output beats closely aligned with the pattern onset beats. However, additional peaks induced by the Tactus Layer are evident, particularly between the third and fourth digits in Fig. 7(A.d) and Fig. 7(B.d), where a cluster of tactus beats emerges.

Comparison of Brain and Motor Layer Neural Activity

The Motor Layer structure can be modeled as a system of coupled oscillators operating at various frequencies, akin to the dynamics of human neural circuits. To analyze neural activity, we compare our results with human EEG recordings

across three rhythmic patterns: a march ('10'), a waltz ('100'), and a broader pattern ('1000') [56], [30]. However, a key distinction between our work and prior studies is that in the latter, participants are pre-trained using 200 ms tatum patterns, leading to a consistent peak in the spectral power at the 200 ms tatum position within the beta-band. In contrast, our approach does not provide the tatum explicitly; rather, the model determines it autonomously, meaning the Inter-Beat Interval (IBI) is not strictly fixed at 200 ms. For an IBI of 400 ms, the model does not require the addition of extra beats to make the prediction, producing a spectrum similar to that found in [30]. For longer IBIs, the model selects alternative tatum positions around 300 ms and 400 ms, respectively. While the reference study reports increased beta activity at the onset and tatum positions, our results in Fig. 8 show that, although the tatum differs, the effect remains similar—beta activity increases at both the onsets and the tatum positions.

Additionally, we refer to the work of [57] and [?], where the authors investigate beta-band activity when 10% of the peaks are missing in an isochronic rhythm. Their EEG results demonstrate that beta-band activity generates expectations for the missing beats. We hypothesize that the 101000 pattern will yield similar results. The findings, shown in Fig. 9 for three frequencies, support this hypothesis. Specifically, for the higher frequencies of 100 BPM and 140 BPM, beta-band activity increases prior to the onset stimuli, with the missing beat occurring on the third beat. When the frequency slows to 60 BPM, the model's beta-band activity is also activated between the two onsets, as well as in response to the missing

onset.

V. CONCLUSION

In this study, we proposed a biologically-inspired hierarchical dynamic system designed to simulate human-like rhythmic cognition. By integrating predictive coding, our model aligns closely with observed human behavior, enhancing its biological plausibility. The physical system offers greater transparency, making it more interpretable and grounded in biological principles. Each layer of the model reflects human-like perception of patterns and frequencies, capturing the intricacies of rhythmic cognition across a wide range of stimuli. The model demonstrates impressive performance in adapting with minimal steps, particularly in its ability to capture the smallest time units. The Tactus Layer successfully mirrors human preference for meter, while the Motor Layer benefits from the higher cognitive layers' decisions at each tatum beat. This hierarchical interaction enables accurate prediction of subsequent beats, while still maintaining human-like variability and errors in beat perception. Furthermore, the Motor Layer's beta-band neuronal activity shows notable similarities to human participants' brain activity in several studies. These results suggest that our model provides a robust framework for understanding rhythmic cognition and offers a promising approach for future research in this domain.

REFERENCES

- [1] C. V. Buhusi and W. H. Meck, "What makes us tick? functional and neural mechanisms of interval timing," *Nature reviews neuroscience*, vol. 6, no. 10, pp. 755–765, 2005.
- [2] J. London, *Hearing in time: Psychological aspects of musical meter*. Oxford University Press, 2012.
- [3] A. D. Patel and J. R. Iversen, "The evolutionary neuroscience of musical beat perception: the action simulation for auditory prediction (asap) hypothesis," *Frontiers in systems neuroscience*, vol. 8, p. 57, 2014.
- [4] E. W. Large and C. Palmer, "Perceiving temporal regularity in music," *Cognitive science*, vol. 26, no. 1, pp. 1–37, 2002.
- [5] A. Breska and R. B. Ivry, "Context-specific control over the neural dynamics of temporal attention by the human cerebellum," *Science Advances*, vol. 6, no. 49, p. eabb1141, 2020.
- [6] S. Proksch, D. C. Comstock, B. Médé, A. Pabst, and R. Balasubramaniam, "Motor and predictive processes in auditory beat and rhythm perception," *Frontiers in Human Neuroscience*, vol. 14, p. 578546, 2020.
- [7] L. Fontolan, B. Morillon, C. Liegeois-Chauvel, and A.-L. Giraud, "The contribution of frequency-specific activity to hierarchical information processing in the human auditory cortex," *Nature communications*, vol. 5, no. 1, p. 4694, 2014.
- [8] J. P. Rauschecker and B. Tian, "Mechanisms and streams for processing of "what" and "where" in auditory cortex," *Proceedings of the National Academy of Sciences*, vol. 97, no. 22, pp. 11 800–11 806, 2000.
- [9] Y. Ito, T. I. Shiramatsu, N. Ishida, K. Oshima, K. Magami, and H. Takahashi, "Spontaneous beat synchronization in rats: Neural dynamics and motor entrainment," *Science Advances*, vol. 8, no. 45, p. eabo7019, 2022.
- [10] D. Bendor and X. Wang, "The neuronal representation of pitch in primate auditory cortex," *Nature*, vol. 436, no. 7054, pp. 1161–1165, 2005.
- [11] R. J. Zatorre, "Pitch perception of complex tones and human temporal-lobe function," *The Journal of the Acoustical Society of America*, vol. 84, no. 2, pp. 566–572, 1988.
- [12] R. D. Patterson, S. Uppenkamp, I. S. Johnsrude, and T. D. Griffiths, "The processing of temporal pitch and melody information in auditory cortex," *Neuron*, vol. 36, no. 4, pp. 767–776, 2002.
- [13] P. A. Lewis and R. C. Miall, "Distinct systems for automatic and cognitively controlled time measurement: evidence from neuroimaging," *Current opinion in neurobiology*, vol. 13, no. 2, pp. 250–255, 2003.
- [14] K. Sakai, O. Hikosaka, and K. Nakamura, "Emergence of rhythm during motor learning," *Trends in cognitive sciences*, vol. 8, no. 12, pp. 547–553, 2004.
- [15] S. W. Kennerley, K. Sakai, and M. Rushworth, "Organization of action sequences and the role of the pre-sma," *Journal of neurophysiology*, vol. 91, no. 2, pp. 978–993, 2004.
- [16] M. Ohbayashi, "The roles of the cortical motor areas in sequential movements," *Frontiers in Behavioral Neuroscience*, vol. 15, p. 640659, 2021.
- [17] P. Janata and S. T. Grafton, "Swinging in the brain: shared neural substrates for behaviors related to sequencing and music," *Nature neuroscience*, vol. 6, no. 7, pp. 682–687, 2003.
- [18] R. I. Schubotz and D. Y. von Cramon, "Functional-anatomical concepts of human premotor cortex: evidence from fmri and pet studies," *Neuroimage*, vol. 20, pp. S120–S131, 2003.
- [19] A. J. Zimmik and M. M. Churchland, "Independent generation of sequence elements by motor cortex," *Nature neuroscience*, vol. 24, no. 3, pp. 412–424, 2021.
- [20] J. J. Cannon and A. D. Patel, "How beat perception co-opts motor neurophysiology," *Trends in Cognitive Sciences*, vol. 25, no. 2, pp. 137–150, 2021.
- [21] P. Hsu, E. A. Ready, and J. A. Grahn, "The effects of parkinson's disease, music training, and dance training on beat perception and production abilities," *PLoS One*, vol. 17, no. 3, p. e0264587, 2022.
- [22] S. L. Bengtsson, H. H. Ehrsson, H. Forssberg, and F. Ullén, "Dissociating brain regions controlling the temporal and ordinal structure of learned movement sequences," *European Journal of Neuroscience*, vol. 19, no. 9, pp. 2591–2602, 2004.
- [23] T.-H. Z. Cheng, S. C. Creel, and J. R. Iversen, "How do you feel the rhythm: Dynamic motor-auditory interactions are involved in the imagination of hierarchical timing," *Journal of Neuroscience*, vol. 42, no. 3, pp. 500–512, 2022.
- [24] V. de Lafuente, M. Jazayeri, H. Merchant, O. García-Garibay, J. Cadena-Valencia, and A. M. Malagón, "Keeping time and rhythm by internal simulation of sensory stimuli and behavioral actions," *Science Advances*, vol. 10, no. 2, p. eadh8185, 2024.
- [25] J. L. Chen, V. B. Penhune, and R. J. Zatorre, "Moving on time: brain network for auditory-motor synchronization is modulated by rhythm complexity and musical training," *Journal of cognitive neuroscience*, vol. 20, no. 2, pp. 226–239, 2008.
- [26] B. Morillon, C. E. Schroeder, and V. Wyart, "Motor contributions to the temporal precision of auditory attention," *Nature communications*, vol. 5, no. 1, p. 5255, 2014.
- [27] T. Braun Janzen, Y. Koshimori, N. M. Richard, and M. H. Thaut, "Rhythm and music-based interventions in motor rehabilitation: current evidence and future perspectives," *Frontiers in human neuroscience*, vol. 15, p. 789467, 2022.
- [28] E. W. Large, I. Roman, J. C. Kim, J. Cannon, J. K. Pazdera, L. J. Trainor, J. Rinzel, and A. Bose, "Dynamic models for musical rhythm perception and coordination," *Frontiers in Computational Neuroscience*, vol. 17, p. 1151895, 2023.
- [29] K. B. Doelling and D. Poeppel, "Cortical entrainment to music and its modulation by expertise," *Proceedings of the National Academy of Sciences*, vol. 112, no. 45, pp. E6233–E6242, 2015.
- [30] H. Merchant, J. Grahn, L. Trainor, M. Rohrmeier, and W. T. Fitch, "Finding the beat: a neural perspective across humans and non-human primates," *Philosophical Transactions of the Royal Society B: Biological Sciences*, vol. 370, no. 1664, p. 20140093, 2015.
- [31] T. Fujioka, B. Ross, and L. J. Trainor, "Beta-band oscillations represent auditory beat and its metrical hierarchy in perception and imagery," *Journal of Neuroscience*, vol. 35, no. 45, pp. 15 187–15 198, 2015.
- [32] P. Vuust and M. A. Witek, "Rhythmic complexity and predictive coding: a novel approach to modeling rhythm and meter perception in music," *Frontiers in psychology*, vol. 5, p. 1111, 2014.
- [33] S. Brown and J. Jordania, "Universals in the world's musics," *Psychology of Music*, vol. 41, no. 2, pp. 229–248, 2013.
- [34] E. W. Large and J. S. Snyder, "Pulse and meter as neural resonance," *Annals of the New York Academy of Sciences*, vol. 1169, no. 1, pp. 46–57, 2009.
- [35] C. E. Schroeder and P. Lakatos, "Low-frequency neuronal oscillations as instruments of sensory selection," *Trends in neurosciences*, vol. 32, no. 1, pp. 9–18, 2009.
- [36] O. Abbasi and J. Gross, "Beta-band oscillations play an essential role in motor-auditory interactions," *Human brain mapping*, vol. 41, no. 3, pp. 656–665, 2020.

- [37] J. A. Grahn and M. Brett, "Rhythm and beat perception in motor areas of the brain," *Journal of cognitive neuroscience*, vol. 19, no. 5, pp. 893–906, 2007.
- [38] J. Ross, J. Iversen, and R. Balasubramaniam, "Dorsal premotor contributions to auditory rhythm perception: Causal transcranial magnetic stimulation studies of interval, tempo, and phase," *bioRxiv*, p. 368597, 2018.
- [39] M. Rosso, B. Moens, M. Leman, and L. Moumdjian, "Neural entrainment underpins sensorimotor synchronization to dynamic rhythmic stimuli," *NeuroImage*, vol. 277, p. 120226, 2023.
- [40] K. Miyazaki, Y. Hiraga, M. Adachi, Y. Nakajima, and M. Tsuzaki, "The beat alignment test (bat): Surveying beat processing abilities in the general population," in *Proceedings of the 10th international conference on music perception and cognition*, 2008.
- [41] M. C. Van Der Steen and P. E. Keller, "The adaptation and anticipation model (adam) of sensorimotor synchronization," *Frontiers in human neuroscience*, vol. 7, p. 253, 2013.
- [42] C. Palmer and A. P. Demos, "Are we in time? how predictive coding and dynamical systems explain musical synchrony," *Current Directions in Psychological Science*, vol. 31, no. 2, pp. 147–153, 2022.
- [43] F. L. Bouwer, C. M. Werner, M. Knetemann, and H. Honing, "Disentangling beat perception from sequential learning and examining the influence of attention and musical abilities on erp responses to rhythm," *Neuropsychologia*, vol. 85, pp. 80–90, 2016.
- [44] A. Celma-Miralles, R. F. De Menezes, and J. M. Toro, "Look at the beat, feel the meter: top-down effects of meter induction on auditory and visual modalities," *Frontiers in human neuroscience*, vol. 10, p. 108, 2016.
- [45] E. Geiser, M. Notter, and J. D. Gabrieli, "A corticostriatal neural system enhances auditory perception through temporal context processing," *Journal of Neuroscience*, vol. 32, no. 18, pp. 6177–6182, 2012.
- [46] S.-J. Kung, J. L. Chen, R. J. Zatorre, and V. B. Penhune, "Interacting cortical and basal ganglia networks underlying finding and tapping to the musical beat," *Journal of cognitive neuroscience*, vol. 25, no. 3, pp. 401–420, 2013.
- [47] T. E. Matthews, M. A. Witek, T. Lund, P. Vuust, and V. B. Penhune, "The sensation of groove engages motor and reward networks," *NeuroImage*, vol. 214, p. 116768, 2020.
- [48] J. A. Grahn and J. B. Rowe, "Feeling the beat: premotor and striatal interactions in musicians and nonmusicians during beat perception," *Journal of Neuroscience*, vol. 29, no. 23, pp. 7540–7548, 2009.
- [49] S. Teki, M. Grube, and T. D. Griffiths, "A unified model of time perception accounts for duration-based and beat-based timing mechanisms," *Frontiers in integrative neuroscience*, vol. 5, p. 90, 2012.
- [50] B. Mathias, A. Zamm, P. G. Gianferrara, B. Ross, and C. Palmer, "Rhythm complexity modulates behavioral and neural dynamics during auditory-motor synchronization," *Journal of Cognitive Neuroscience*, vol. 32, no. 10, pp. 1864–1880, 2020.
- [51] O. A. Heggli, J. Cabral, I. Konvalinka, P. Vuust, and M. L. Kringelbach, "A kuramoto model of self-other integration across interpersonal synchronization strategies," *PLoS computational biology*, vol. 15, no. 10, p. e1007422, 2019.
- [52] M. Rosso, M. Leman, and L. Moumdjian, "Neural entrainment meets behavior: the stability index as a neural outcome measure of auditory-motor coupling," *Frontiers in Human Neuroscience*, vol. 15, p. 668918, 2021.
- [53] P. Berens, "Circstat: a matlab toolbox for circular statistics," *Journal of statistical software*, vol. 31, pp. 1–21, 2009.
- [54] K. Cho, "Learning phrase representations using rnn encoder-decoder for statistical machine translation," *arXiv preprint arXiv:1406.1078*, 2014.
- [55] B. Lim, S. Ö. Arık, N. Loeff, and T. Pfister, "Temporal fusion transformers for interpretable multi-horizon time series forecasting," *International Journal of Forecasting*, vol. 37, no. 4, pp. 1748–1764, 2021.
- [56] T. Fujioka, L. J. Trainor, E. W. Large, and B. Ross, "Internalized timing of isochronous sounds is represented in neuromagnetic beta oscillations," *Journal of Neuroscience*, vol. 32, no. 5, pp. 1791–1802, 2012.
- [57] A. Chang, D. J. Bosnyak, and L. J. Trainor, "Rhythmicity facilitates pitch discrimination: Differential roles of low and high frequency neural oscillations," *NeuroImage*, vol. 198, pp. 31–43, 2019.